Drug nanoparticles by emulsion-freeze-drying via the employment of branched block copolymer nanoparticles

Ulrike Wais[a,b,†], Alexander W. Jackson[b,†], Yanming Zuo[c], Yu Xiang[c], Tao He*[c], Haifei Zhang*[a]

[a] Department of Chemistry, University of Liverpool, Liverpool, L69 7ZD, UK

[b] Institute of Chemical and Engineering Science, 1 Pesek Road, Jurong Island, 627833, Singapore

[c] School of Chemistry and Chemical Engineering, Hefei University of Technology, Hefei, China.

† Equal contribution

* Corresponding authors: zhanghf@liv.ac.uk (HZ), taohe@hfut.edu.cn (TH)

Abstract: A large percentage of drug compounds exhibit low water solubility and hence low bioavailability and therapeutic efficacy. This may be addressed by preparation of drug nanoparticles, leading to enhanced dissolution rate and direct use for treatment. Various methods have been developed to produce drug nanocrystals, including wet milling, homogenization, solution precipitation, emulsion diffusion, and the recently developed emulsion freeze-drying. The drawback for these methods may include difficult control in particles size, use of surfactants & polymer, and low ratio of drug to stabilizer. Here, biocompatible branched block copolymer nanoparticles with lightly-crosslinked hydrophobic core and hydrophilic surface groups are synthesized by the direct monomer-to-particle methodology, characterized, and then used as scaffold polymer/surfactant to produce drug nanoparticles via the emulsion-freeze-drying approach. This method can be used for model organic dye and different poorly water-soluble drugs. Aqueous drug nanoparticles dispersions can be obtained with high ratio of drug to stabilizer and relatively uniform nanoparticle sizes.

1. Introduction

A report published in 1988 demonstrated that of all pharmaceutical drugs produced in the UK over a timeframe of 20 years, 40% exhibited poor bioavailability[1]. New and improved screening methods can now predict and eliminate some drug candidates with low bioavailability, before going into testing[2]. Still a report published in 2004[3] reported that only 17.1% of all *essential drugs* defined by the world health organisation (WHO) could be classified as BCS II drugs (high permeability and low solubility) and 10.6% as BCS IV drugs (low permeability and low solubility), as defined by Amidon and co-workers[4]. Low bioavailability is the direct consequence of low water solubility for a large percentage of drugs, particularly for BCS II drugs. A promising approach to enhance solubility of poorly water-soluble drugs is nanosizing technologies, with the particle sizes in the range of 10 to 1000 nm[5]. Reducing particle size to nanoscale range enhances both the saturation solubility as described in the Oswald-Freundlich equation[6, 7] and the dissolution rate as shown in the Noyes-Whitney equation[8].

Both top-down and bottom-up routes have been reported to form nanoparticles. In the top-down process, larger drug particles are downsized by mechanical methods, e.g., grinding (wet-media milling)[9-12], or by the application of pressure (Piston-Gap)[13-15]. Top-down processes, although used more in industry[16], have disadvantages of being time and energy inefficient, difficult to produce small nanocrystals and control particle size distribution, and not applicable for hard crystalline drugs without pre-treatment. More than one cycle of operation is often required, prone to introducing impurities from solvent or milling material[17, 18]. In bottom-up processes the nanoparticles are formed from solution, whereby a better control of the crystallisation process can lead to smaller particles with narrower particle size distribution. The main obstacle in bottom-up approach is repressing and stabilizing against Ostwald-Ripening. A variety of bottom-up methods have been described and excellent reviews can be found accordingly [18, 19]. Established and industrially applied approaches [19] include solvent-antisolvent precipitation (SAS)[20-22], with its variation of high gravity reactive precipitation (HGRP)[23, 24], supercritical fluid precipitation[25-28] and spray drying[29-31]. Although these techniques have certain advantages, like easy handling

(SAS), almost no solvent residue (supercritical fluid) and are more cost and energy efficient, problems in stabilizing particle suspensions remain. A solution to this problem, while still maintaining the advantages of bottom-up processes, is to rapidly freeze the drug solution and arrest particle growth due to freezing. In freeze-drying a solution is frozen and the solvent is subsequently removed in a freeze-dryer under vacuum [32-34]. In spray freeze drying, the dissolved material is sprayed into liquid nitrogen for downsizing and subsequently freeze dried. This is mainly used for preparation of protein particles, which would denature under harsh conditions [35-37].

We previously reported the use of emulsion freeze-drying to form organic or drug nanoparticles *in situ* in water-soluble porous polymer. The polymer scaffold prevents the nanoparticles from aggregation in the solid state, ensuring a long storage time. The nanoparticles can be readily released by dissolving the polymer scaffold in water to produce aqueous nanoparticle dispersion[38]. Both polymer (*e.g.*, poly(vinyl alcohol)) and surfactant (*e.g.*, sodium dodecyl sulphate) are required to form the emulsions, produce the porous scaffold, and stabilize the nanoparticles in aqueous suspensions. It is possible to generate porous polymer by freeze drying and then employ a solvent evaporation approach to form organic/drug nanoparticles directly in the porous polymeric scaffold [39, 40]. Aqueous nanoparticles dispersion can be prepared similarly. In both approaches, the use of both polymer and surfactant is important in forming stable aqueous nanoparticle dispersions. This, however, can result in low loading of drug compounds in the formulations. A formulation that utilizes a biocompatible polymer acting both as scaffold and surfactant would be advantageous in improving drug loading and reducing the formulation complexity (*e.g.*, in assessing biocompatibility).

We have also reported synthesis of super-lightly crosslinked branched copolymers and a new *direct* monomer-to-particle synthetic strategy based on these copolymers, which could be applied in drug delivery [41-43]. After a simple dialysis process to generate isolated *macromolecular species*, well-defined uni-molecular polymer nanoparticles can be obtained directly. This *de novo* synthetic approach differs significantly from the reported arm-first or core-first core-crosslinked star-polymer synthesis where the core is effectively a highly cross-linked microgel formed by the addition of a large volume of cross-linkers such as divinylbenzene at the end of the polymerisation [44-46]. In contrast, polymer nanoparticles were prepared from discrete soluble molecular species (soluble

branched copolymers) which have been synthesized by a controlled branching strategy. Utilizing this strategy, it was possible to prepare amphiphilic materials with defined nanoparticle shape by a one-pot, concerted growth process rather than joining of pre-formed spheres [41, 42]. The lightly crosslinked core could offer the obtained polymer nanoparticles with larger loading capacity of guest compounds. And the stability of the nanoparticles was very high (*e.g.*, up to one year maintaining the size and shape). This synthetic methodology may be easily scaled-up as we demonstrated previously, even with the possibility to be extended in the synthesis of hyperbranched polydendrons [47].

Herein, we demonstrated for the first time that the branched copolymer nanoparticles (BCN) could be used to form stable emulsions without other additives. The branched copolymers applied here were the biocompatible poly(ethylene glycol)-b-(*N*-isopropylacrylamide) (PEG-PNIPAM). The formed oil-in-water (O/W) emulsions with hydrophobic dyes or drug compounds dissolved in the oil-droplet phase were freeze-dried to form nanoparticles *in situ* within the PEG-PNIPAM scaffold, which can then be readily dissolved in water to produce aqueous nanoparticles dispersions.

2. Experimental

2.1 Chemicals and reagents

Deionized water was prepared using an AquaMAX-Basic 321 DI water purification system. Oil Red O (OR) dye content ≥ 75%, ketoprofen ≥ 98% (TLC), ibuprofen ≥ 98% (HPLC), indomethacin ≥ 99% (TLC), *o*-xylene ≥ 98% (GC), sodium acetate, *N*-isopropylacrylamide (NIPAM, 97%), and dodecanethiol (98%) were purchased from Sigma-Aldrich. Macro-azo poly(ethylene glycol) initiator was obtained from Wako Pure Chemical Industries Ltd (Osaka, Japan). Cyclohexane (extra pure) and *o*-xylene were purchased from Fisher scientific and VWR international respectively. All other solvents were reagent grade and purchased from Sigma-Aldrich. All chemicals were used as received.

2.2 Synthesis of crosslinked branched poly(ethylene glycol)-b-Poly(N-isopropylacrylamide) (PEG-PNIPAM)

2.2.1 Synthesis of ethylene diacrylamide

Ethylene diamine (1.2 g, 20 mmol, 1 eq) and sodium acetate (3.6 g, 40 mmol, 2 eq) were dissolved in $CHCl_3$ (50 mL) and the solution cooled to 0 ºC in an ice bath. Acryloyl chloride (3.6 g, 44 mmol, 2.2 eq) in $CHCl_3$ (50 mL) was then added dropwise over 20 mins. The reaction was left to stir for 1 h at 0 ºC. The reaction was then refluxed for 1 h at 60 ºC and the solution filtered while hot, upon cooling a white precipitate formed which was isolated by filtration. The crude white solid was further purified by recrystallization in hot $CHCl_3$ to afford the desired product ethylene diacrylamide as a white solid (1.2 g, 36 %). ^{1}H NMR (DMSO-d_6): δ 8.19 (s, 2H), 6.19 (m, 2H), 6.07 (m, 2H), 5.58 (m, 2H), 3.21 (m, 4H). ^{13}C NMR (DMSO-d_6): δ 164.9, 131.8, 125.2, 38.4. HRMS (ESI) *m*/*z*: $[M + H]^+$ calculated for $C_8H_{13}N_2O_2$, 169.0972; found: 169.0980 (ppm 4.77).

*2.2.2 Synthesis of PEG-PNIPAM (**1**-**3**) and the corresponding nanoparticle dispersions*

Typically, the radical macro-initiator poly(ethylene glycol) dimer (12 kDa, 1.2 g, 0.1 mmol, 1 eq), *N*-isopropylacrylamide (0.56 g, 5 mmol, 25 eq per PEG chain), ethylene diacrylamide (10.1 mg, 0.06 mmol, 0.3 eq per PEG chain) and dodecanethiol (10.1 mg, 0.05 mmol, 0.25 eq per PEG chain) were transferred into a small schlenk tube fitted with a magnetic stirrer bar and *N*,*N*'-dimethylformamide (DMF,7 mL) added. The reaction mixture was degassed and the vessel was backfilled with N_2. The reaction mixture was then placed in an oil bath at 70 °C and the polymerization was quenched by rapid cooling after 16 h. The reaction mixture was dissolved in a minimal amount of tetrahydrofuran (THF) and added dropwise to a large excess of ice-cold diethyl ether. The precipitation was repeated once more before the desired branched copolymer was obtained as a white solid (0.94 g). The molar ratio of ethylene diacrylamide per PEG chain was varied as 0.3 (**1**), 0.6 (**2**), and 0.9 (**3**) eq per PEG change for the PEG-PNIPAM branched block copolymers. Corresponding nanoparticles aqueous suspension can be prepared by a simple solvent-removal process. Typically, 10 mg of branched block copolymer was dissolved in 5 mL of acetone, followed by addition of 5 mL of water and stirred for

0.5 h at room temperature. Acetone was removed by evaporation at room temperature, and final transparent nanoparticles aqueous suspension was obtained.

2. 3 Formulation of nanoparticles by emulsion-freeze-drying approach

Stock solutions of 2 wt% branched block polymer PEG-PNIPAM (0.3, 0.6 and 0.9 cross-linkages as synthesized by ethylene diacrylamide of 0.3, 0.6, 0.9 eq per PEG chain) in deionized water and 0.5 wt% Oil Red O (or indomethacin, ibuprofen, ketoprofen) in cyclohexane (*o*-xylene) solutions were prepared. Cyclohexane and *o*-xylene were chosen as the organic solvents to dissolve the hydrophobic dye/drugs because they are Class 2 solvents for pharmaceuticals with high concentration limits (3880 ppm and 2170 ppm, respectively) [48]. Both solvents are volatile with high melting points (~ 4 ºC for cyclohexane and - 25 ºC for *o*-xylene), which makes them suitable for a freeze-drying process. Furthermore, both solvents could be readily emulsified to form stable oil-in-water emulsions [38, 49]. Solvent residuals after freeze-drying could be within the limit as defined by the International Council for Harmonization of Technical Requirements for Pharmaceuticals for Human Use (ICH) as shown by freeze-drying organic solvents with similar vapour pressure [50]. Under stirring at 1000 rpm with an overhead stirrer (Eurostar digital, IKA-WERKE), the cyclohexane solution was added dropwise over a period of 2 minutes to the aqueous PEG-PNIPAM solution at room temperature (also once at 50 °C to investigate the temperature effect because the NIPAM block is known to be temperature sensitive). The emulsions with the volume ratios of aqueous phase to organic phase (W/O) of 1:4; 1:3 and 1:2 were prepared. After continuously stirring for 2 minutes at 1000 rpm, the emulsions were homogenized for another 2 minutes using a Power Gen 1000 homogenizer by Fischer Scientific on setting 3. This was to produce the emulsion with smaller droplets. The emulsion was rapidly frozen in liquid nitrogen and placed in a CoolSafe freeze dryer by Scanvac at a condensing temperature of -90 °C and lyophilized for two days to produce dry porous polymer containing organic nanoparticles.

2. 4 Characterisation

The emulsions were imaged on an Olympus CX41 microscope with Plan magnifying lenses. CellSens entry imaging software by Olympus was used for size measurements. ^{1}H and ^{13}C NMR spectra were

recorded on Bruker 400 Ultra Shield spectrometer. High resolution mass spectrometry was performed on a Thermo Finnigan MAT 95XP HRSM spectrometer. Particle size and Zeta-Potential was measured by dynamic laser scattering (DLS) analysis on a Malvern Zetasizer Nanoseries at 25 °C from Malvern Instruments. Polydispersity index (PDI) was obtained from Malvern software, indicating the particle size distribution. PDI values greater than 0.7 would indicate a very broad particle size distribution and the DLS method might not be suitable. The measurements were performed on aqueous nanoparticles suspensions with concentrations of 0.5 mg/ml. Microparticles or aggregates were removed by centrifugation with an Eppendorf Centrifuge 5415 D at 3000 rpm for 3 minutes and one minute at 3600 rpm to ensure that larger particles precipitate.

Scanning electron microscope (SEM) images were obtained using a Hitachi S-4800 SEM. The samples were coated with gold prior to imaging on an Emitech K550X Automated Sputter Coater. The freeze-dried samples were cut into thin slices and carefully mounted to the SEM stud using double adhesive carbon tape. For aqueous nanoparticles suspension, a drop of the suspension was deposited on a clean SEM stud and the solvent was left to evaporate before coating with gold. The cyro-transmission electron microscopic (cryo-TEM) analysis was performed on Tecnai G2 Spirit - T12 with 120 kV acceleration made by FEI, Hillsboro, USA. Powder x-ray diffraction (PXRD) data was collected on a PanalayticalX'Pert Pro Multi-Purpose Diffractometer in high-throughput transmission geometry. Cu Kα Radiation was used with Λ=1.541 Å and a divergence slit of 0.76 mm. Samples were pressed in a well of an aluminium plate and scanned at 40 kV and 40 mA over 5-50 ° 2θ with a scan time of 60 min and a step size of 0.0131°.

2. 5 Determination of the nanoparticles yields in the formulations

5 mg of freeze dried material was dispersed in 10 mL deionized water and centrifuged at 3000 rpm for 3 minutes and another minute at 3600 rpm with an Eppendorf Centrifuge 5415 D. This was to precipitate the larger particles by centrifuging and the nanoparticles remained in the supernatant solution. The precipitant was redissolved in ethanol. The concentrations of Oil Red O (OR) or other drug compounds were determined by UV/Vis absorption on a µQuant spectrometer by Northstar Scientific. Ethanol was added to the aqueous supernatant and water was then added to the ethanol

solution of precipitation to achieve a 1:1 v/v ethanol/water mixture. The measured absorption was compared to a standard curve of OR (or indomethacin) in the 1:1 v/v ethanol/water medium. Yield of ketoprofen and ibuprofen was measured on a 1200 series HPLC (because of no UV absorbance on the UV-Vis spectrum) from Agilent, comprising a vacuum degasser, quaternary pump, ALS auto-sampler, heated column compartment and UV-Vis detector. A 300 mm by 4.6 mm phase symmetry silica column with a particle diameter of 5 µm and a pore size of 120 Å was used. A flow rate of 1 ml/min was set. The mobile phase was a mixture of hexane and isopropyl alcohol with 70 v/v % hexane for ketoprofen and 90% hexane for ibuprofen. All tests were carried out at 20 °C. All signals were UV detected at 254 nm. Data analysis was performed using Agilent Chemstation software, version B.02.01 (Agilent Technologies, USA).

Nanoparticle yield was calculated using the following equation:

$$Yield = \frac{m_{NP}}{m_T} \times 100 = \frac{m_S}{m_S + m_P} \times 100$$

Where m_{NP} is the mass of nanoparticles and m_T the total mass of drug. The nanoparticle mass is measured from the supernatant phase after centrifuging (m_S). m_P indicates the mass of the drug or OR found in the precipitant. Initial tests showed that PEG-PNIPAM was not UV active and did not affect absorption of OR or the relevant drug compounds on the UV-Vis spectra.

3. Results and discussion

3.1 Synthesis of PEG-PNIPAM and the polymer nanoparticles

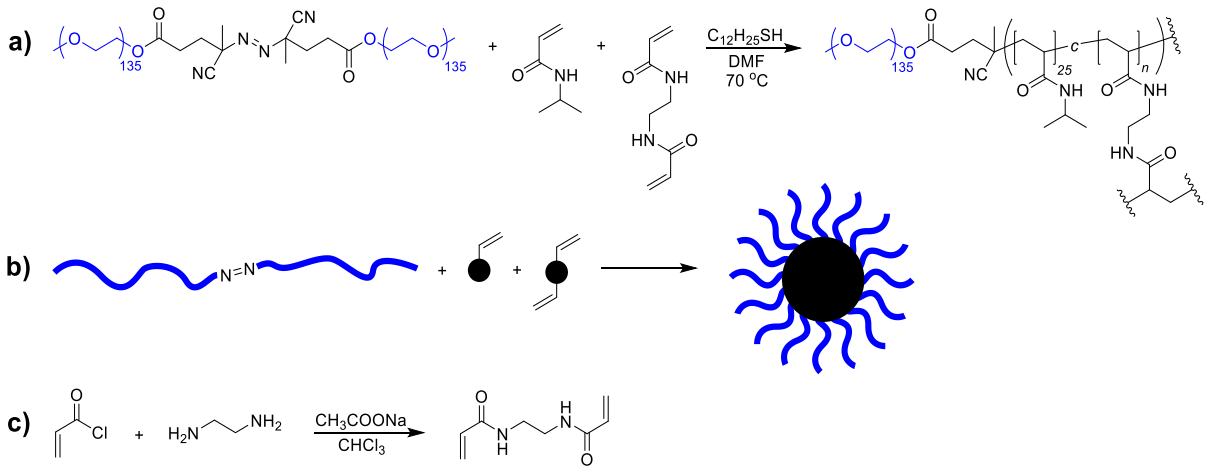

Fig. 1 Preparation of lightly crosslinked branched copolymer poly(ethylene glycol)-b-(*N*-isopropylacrylamide). (a) Synthesis of branched copolymer of poly(ethylene glycol)-b-(*N*-isopropylacrylamide) using poly(ethylene glycol) dimer macro-azo initiator with ethylene diacrylamide as crosslinker in presence of dodecanethiol at 70 °C in DMF; (b) Cartoon representation of the branched copolymer synthetic procedure; (c) Synthesis of small molecular diacrylaimde crosslinker of ethylene diacrylamide.

Previously, atom transfer radical polymerization (ATRP) has been employed to synthesize branched copolymers together with the nanoparticles preparation [41,42]. Herein, in order to synthesize biocompatible nanoparticles with more convenience and high potential of scaling-up for future clinic applications, we have developed a much easier method by using macro-azo PEG initiator in presence of chain transfer agent for the synthesis of biocompatible branched AB block copolymer PEG-PNIPAM with varying crosslinking degrees. Three branched PEG-PNIPAM copolymers with varying cross-linking degrees were synthesized. Although conventional radical polymerizations instead of living radical polymerizations was employed, discrete soluble molecular species (soluble branched copolymers) in solvents such as acetone, THF etc. could still be obtained, which suggested the process to be a relatively controlled branching strategy [41,42].

It should be pointed out that when the branched copolymers were dissolved in water directly, clear solution could be obtained, but it was difficult to get a well defined DLS profile. This suggested that

the relatively low Mw PEG (*eg.*, 6000) on the corona could not fully stabilize the uni-branched copolymer nanoparticles, and resulted in dynamic aggregation-disaggregation of single nanoparticles, which is different from our previous reports where the MW of PEG blocks was above 1.2k. In that case, the uni-molecular branched copolymer nanoparticles could be stabilized by the outer PEG chains [41,42]. However, for the PEG-PNIPAM synthesised in this study, after the simple solvent removal process (see experimental section), stable and clear nanoparticles aqueous suspensions with well-defined DLS profiles could be obtained (Fig. 1, Fig. 2, and Table 1).

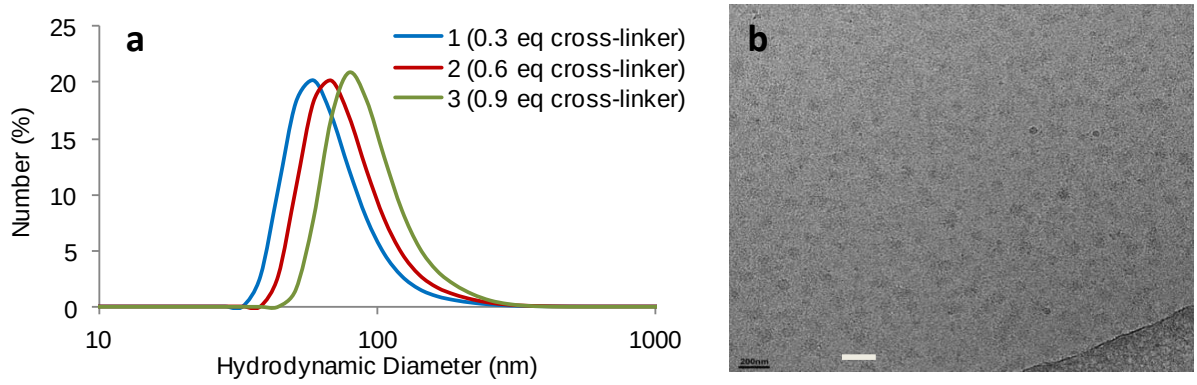

Fig. 2 (a) Dynamic laser scattering analysis of PEG-PNIPAM nanoparticles in H_2O at 25 ºC after the solvent evaporation procedure; (b) Cryo-TEM images of nanoparticles 2 with 0.6 crosslinkage (scale bar: 200nm).

Due to the relatively large size of these nanoparticles in aqueous media and their relatively small polymer building blocks, it is hypothesized that they aggregate into larger architectures comprised of smaller branched PEG-PNIPAM nanoparticles, where there are sufficient PEG chains on the corona to stabilize the nano-aggregates. As the degree of cross-linking increased, a slight increase in aggregate size was observed (Fig. 2). The nanoparticles sizes measured by DLS (number average sizes) were consistent with the sizes observed by cryo-TEM imaging. It was observed that upon heating to temperatures above the lower critical solution temperature (LCST) of *N*-isopropylacrylamide, the nanoparticles further aggregate due to increase in hydrophobicity. The temperature induced aggregation decreased with the increased degree of cross-linking, suggesting that the poly(ethylene glycol) coronal arms are better in shielding the hydrophobic cores.

Table 1 Synthesis of lightly crosslinked branched copolymer PEG-PNIPAM and corresponding nanoparticles with varying amounts of ethylene diacrylamide crosslinker.

Branched Block Copolymers	PEG dimer	NIPAM	ethylene diacrylamide	dodecanethiol	DMF	Temp	Time	size (D_h)
1	0.1 mmol	5 mmol (25 eq per PEG chain)	0.06 mmol (0.3 eq per PEG chain)	0.05 mmol (0.25 eq per PEG chain)	7 mL	70 ºC	16 h	70 nm
2	0.1 mmol	5 mmol (25 eq per PEG chain)	0.12 mmol (0.6 eq per PEG chain)	0.05 mmol (0.25 eq per PEG chain)	7 mL	70 ºC	16 h	81 nm
3	0.1mmol	5 mmol (25 eq per PEG chain)	0.18 mmol (0.9 eq per PEG chain)	0.05 mmol (0.25 eq per PEG chain)	7 mL	70 ºC	16 h	96 nm

3.2 Hydrophobic dye OR nanoparticles by emulsion freeze-drying

Due to their relatively hydrophobic core (hydrophobicity coming from the iso-propyl and C-C bond on side and main chain of PNIPAM) and hydrophilic corona (PEG), the branched PEG-PNIPAM was investigated as stabilizer to form emulsions and then used to produce poorly water-soluble dye and drug nanoparticles by the emulsion-freeze-drying approach. Emulsions are mixtures of two, normally, immiscible liquid phases, with one phase as droplets dispersed in the other continuous phase, and stabilized by surfactants [51]**.** Emulsions may be also formed using colloids as stabilizers, which are called Pickering emulsions [52]**.** In this study, the PEG-PNIPAM nanoparticles in water were used as the stabilizers to form oil-in-water (O/W) emulsions. The subsequent freeze-drying produced organic nanoparticles directly within the porous PEG-PNIPAM. No additional surfactant or polymer was used. This could in principle improve the drug loading in the nanoformulations and also reduce the complexity when evaluating the formulation's cytotoxicity. The OR solution in cyclohexane or indomethacin (or ibuprofen and ketoprofen) solution in *o*-xylene (both concentration 0.5 wt%) were

used to form the emulsions in order to produce the relevant organic nanoparticles. The emulsions with 80, 75 and 66% oil phase were produced with PEG-PNIPAM (1-3).

Oil Red O (OR), an organic dye, was chosen for initial testing because of its low water-solubility and red colour. It was possible to form stable emulsions with 80, 75 and 66% oil phase using 0.3 crosslinked PEG-PNIPAM. Increasing crosslinkage and decreasing oil phase destabilized the emulsions. Hence using 0.6 cross-linked PEG-PNIPAM emulsions with 66% oil phase were not stable, while emulsion formation with 0.9 cross-linked PEG-PNIPAM was possible with 80% oil phase (Table 2). After freeze drying, a highly porous material was obtained [38], that could be easily dissolved in water to form clear red nanosuspension as shown in Fig. 3. This nanosuspension looks like a solution, indicating presence of small nanoparticles which do not diffract the light while the unprocessed OR can only float on the water surface (Fig. 3b-c). DLS measurements showed that the obtained OR particles were between 300 to 500 nm by Z-average (Table 2). During the formation of emulsion, it is hypothesized that on adding the organic solution into the aqueous PEG-PNIPAM solution, the aggregates of single branched copolymer PEG-PNIPAM nanoparticles (which would be much smaller than the nanoparticles formed after solvent evaporation procedure) in water were destroyed and re-dispersed, resulted in the absorption of single or small aggregates of branched copolymer nanoparticles outside the emulsion acting as nano-surfactant and stabilize the whole droplets. After the freeze-drying process, the OR particles were formed in the pores of the porous polymer.

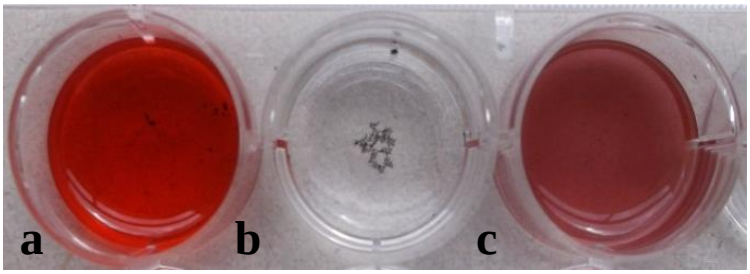

Fig. 3 a) Oil Red O solution in cyclohexane; b) insoluble Oil Red O in water; c) aqueous Oil Red O nanoparticle dispersion.

Table 2 Overview of size, zeta potential and yield of OR nanoparticles prepared by emulsion freeze drying.

Cross linkage	Oil Phase [%]	Z-Average [nm]	Intensity Peak [nm]	PDI	Zeta [mV]	Yield [%]
0.3	80	395	438	0.42	-54 ± 8.29	45
0.3	75	340	980, 274	0.39	-26 ± 4.98	37
0.3	66	423	760,231	0.35	-31 ± 6.71	50
0.6	80	506	606, 115	0.29	-27 ± 6.47	54
0.6	75	298	376	0.22	-18 ± 4	67
0.6	66	not stable	not stable	not stable	not stable	not stable
0.9	80	348	456	0.33	-25 ± 8	36
0.9	75	not stable	not stable	not stable	not stable	not stable
0.9	66	not stable	not stable	not stable	not stable	not stable

No discernible trend in size could be seen, since emulsions for higher cross-linked PEG-PNIPAM could not be obtained. The Z-average sizes of OR nanoparticles shown in Table 2 are heavily dependent on the number of particles. Since larger particles scatter light with more intensity, size is shifted to larger particles in a polydisperse sample [53]. The particle size distribution may be shown by the peak width on DLS profiles, which may be based on scattering intensity or particle number. Fig. 4 shows the DLS plots by intensity. The intensity peak sizes and the relevant polydispersity index (PDI) are included in Table 2 as well. As Z-average only gives a single average number, the intensity profiles could tell more about particle size distribution. To get a clearer picture about particle size distribution, the DLS profiles by particle number were also given in Fig. S1. The average or peak sizes by particle numbers were generally smaller that those by intensity. From both Fig. 4 and Fig. S1, the main particle sizes were around 100 to 300 nm with only a small percentage of

particles being bigger than 300 nm. This was also confirmed by SEM images of the dried nanosuspensions on SEM stud (Fig. 5). Figure 5a, b and c clearly show OR ellipsoid nanoparticles of about 100 to 200 nm.

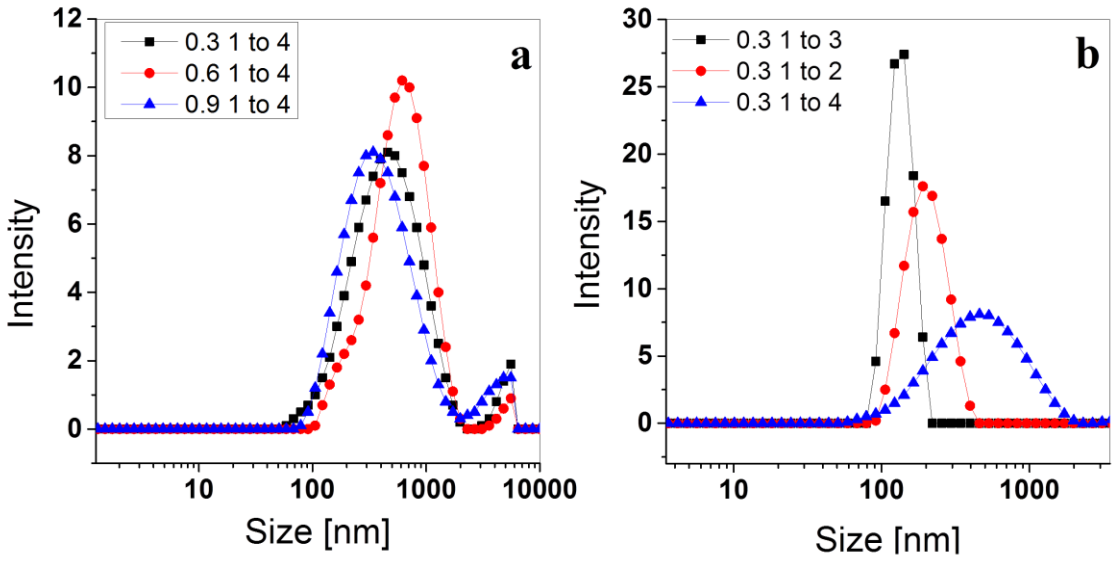

Fig. 4 DLS intensity data of nanosuspensions of a) OR nanosuspensions from different crosslinked PEG-PNIPAM with 80% oil phase (W/O=1/4); b) OR nanosuspensions from 0.3 crosslinked PEG-PNIPAM with varying oil phase percentages (W/O).

Yield of the nanoparticles was calculated using UV/Vis measurement data. To separate microparticles from nanoparticles, the suspensions formed by dissolving the dry materials in water were centrifuged at 3000 rpm for 3 min and at 3600 rpm for another minute. The increase in speed for an additional minute was done to insure that the precipitates settled as a pellet and that the supernatant could easily be removed. Sedimentation of particles by centrifugation is dependent on mass, shape, and suspension medium as postulated by Svedberg et al. [54, 55]. The obtained DLS data of the supernatant as well as the SEM data of the precipitated material (Fig. 5) show that the microparticles precipitated by centrifugation while the nanoparticles remained in the supernatant phase. The achieved yields of 36% - 67% may not be very high but this process required no use of additional surfactants [38].

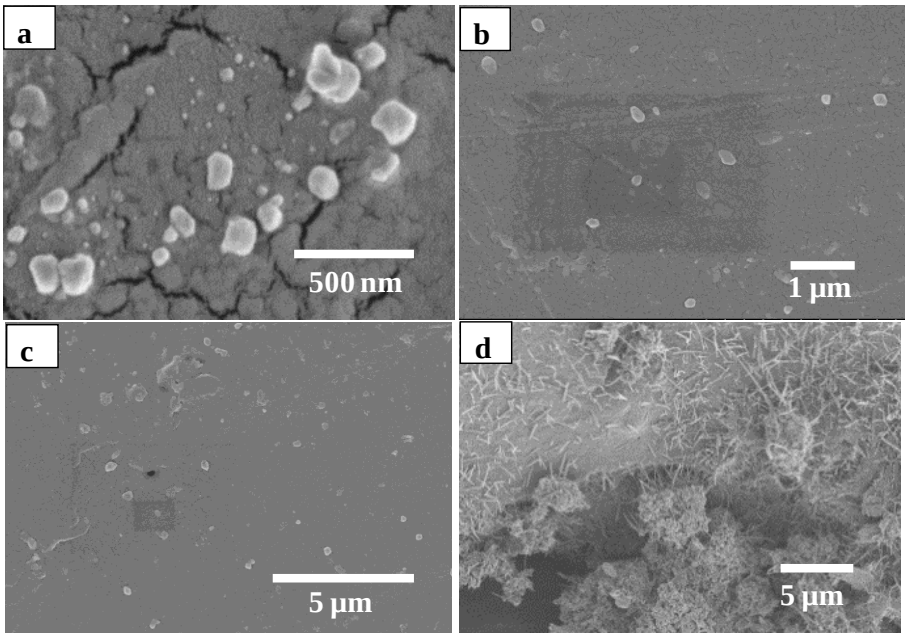

Fig. 5 SEM images of OR nanoparticles prepared from a) 0.3 crosslinked PEG-PNIPAM from emulsions with 75% oil phase; b) 0.6 crosslinked PEG-PNIPAM from emulsions with 75% oil phase; c) 0.9 crosslinked PEG-PNIPAM from emulsions with 75% oil phase and d) the precipitated OR particles after centrifuging sample (a).

Many nanoparticle formulations experience the problem of particle agglomeration after processing, which is often addressed via the use of surfactants as stabilizers [33]. In this work the formed nanoparticles were prevented from aggregation by the porous polymer scaffold shown in Fig. 6. The highly interconnected porous scaffold was a result of emulsion templating and ice templating. Because of the low atomic contrast between OR and the polymer scaffold and the possible encapsulation, it was very difficult to directly observe OR nanoparticles within the polymer scaffold. But the OR nanoparticles were stable in the PEG-PNIPAM matrix because nanoparticle suspensions were still produced after storing the dry materials in desiccator for 8 months (Fig. S2).

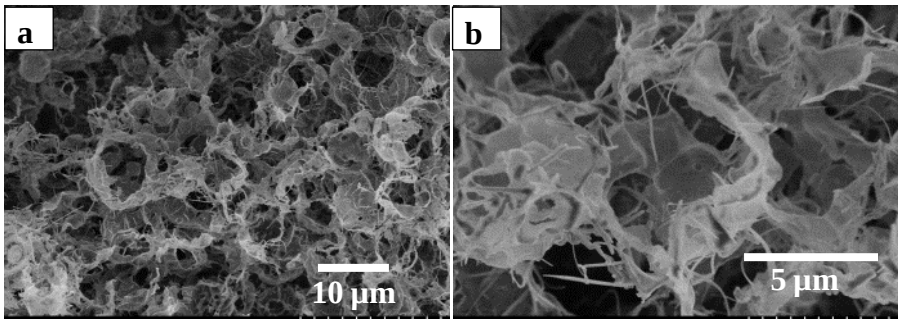

Fig. 6 SEM images of 0.6 crosslinked PEG-PNIPAM scaffolds with OR nanoparticles at different magnifications (a, b). The original emulsion was 75% oil phase.

3.3 Indomethacin nanoparticles by emulsion freeze-drying

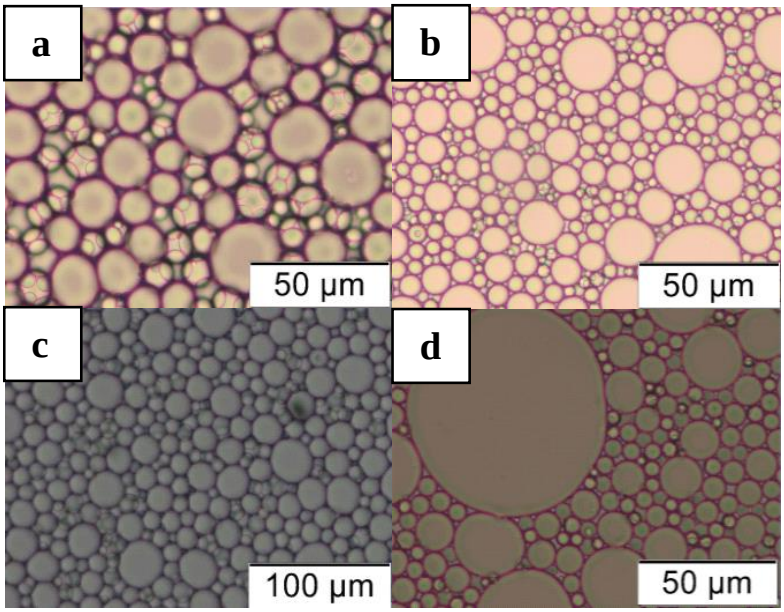

Fig. 7 Optical microscopic images of the emulsions formed by dispersing IMC-xylene solution in aqueous PEG-PNIPAM solution at room temperature unless stated otherwise. a) 0.9 crosslinked PEG-PNIPAM with 75 % oil phase (W/O =1:3); b) 0.9 crosslinked PEG-PNIPAM with 66 % oil phase (W/O =1:2); c) 0.6 crosslinked PEG-PNIPAM with 75 % oil phase (W/O =1:3); and d) 0.9 crosslinked PEG-PNIPAM with 75 % oil phase (W/O =1:3) with the emulsions prepared at 50 °C.

It was possible to extend this approach to the preparation of poorly water soluble drugs. Indomethacine (IMC) was selected as a model drug for this approach as it was investigated before by the emulsion-freeze-drying approach [49]. IMC was dissolved in *o*-xylene and the organic solution was emulsified as the internal phase to form the O/W emulsions. Compared to OR-cyclohexane solution, stable emulsions for all O/W ratios and all crosslinkages of PEG-PNIPAM were formed. Fig. 7 shows optical images of the emulsions with different W:O ratios of 1 to 3 and 1 to 2 (a and b), crosslinkage variation of 0.9 and 0.6 (c and a) and variations in temperature (d). The droplet sizes spanned from 3 µm to 20 µm with the average being around 5 µm. The very large droplets in Fig. 7d

were likely a result of an increasing instability of the emulsion due to the higher preparation temperature at 50 °C. The average droplet size decreased slightly when the volume of oil phase was decreased. The crosslinkage level of PEG-PNIPAM did not seem to have significant influence on droplet size.

Table 3 Overview of size, zeta potential and yield of IMC nanoparticles.

Cross linkage	Oil Phase [%]	Z-Average [nm]	Intensity Peak [nm]	PDI	Zeta [mV]	Yield [%]
0.3	80	480	472	0.22	-17 ± 4	40
0.3	75	475	486	0.18	-11 ± 4	23
0.3	66	484	396, 192	0.36	-18 ± 5	28
0.6	80	551	408	0.35	-14 ± 4	46
0.6	75	476	492, 148	0.51	-13 ± 4	38
0.6	66	552	713, 219	0.43	-14 ± 4	40
0.9	80	454 (1038)*	472, 93	0.33	-11 ± 4 (-16 ± 3)*	53 (38)*
0.9	75	507	545, 163	0.33	-10 ± 3	43
0.9	66	470	484, 112	0.38	- 7 ± 3	64

Note: *emulsion prepared at 50 °C

The size, zeta potential, PDI and yield of IMC nanoparticles are given in Table 3. The IMC yields increased to 64% with increasing crosslinkage. Lower percentage of oil phase in the emulsions led to decrease in nanoparticle yield for 0.3 and 0.6 crosslinked PEG-PNIPAM, while no obvious trend was observed for the 0.9 crosslinked PEG-PNIPAM. The DLS and zeta potential measurements

included three separate runs, from which the average values were calculated and used. The zeta potential exhibited by OR nanoparticle was roughly two times that for IMC nanoparticle. Zeta potential was found to be in the same domain of -10 to -15 mV for IMC and -20 to -30 mV for OR particles. Z-average data showed that IMC nanoparticles with sizes between 450 and 550 nm could be formed. Generally OR particles tended to be smaller in size than IMC particles.

Particle size distributions by intensity (Fig. S3) and by number (Fig. S4) were both measured. The presence of single peak or multiple peaks was the same for the DLS profiles either by intensity or number. However, for polydispersed samples, the shape of the profiles was different. Larger particles generated higher peak intensity in the intensity plot (Fig. S3) while the smaller sized particles gave higher number percentage peak in the number plot (Fig. S4). There was no obvious trend for the impact on particle sizes from ratio of water to oil and polymer crosslinkage. The impact on particle size distribution was quite small as well. It should be mentioned that the IMC nanoparticles within the PEG-PNIPAM scaffold were also highly stable. After the storage of IMC particles-PEG-PNIPAM in desiccator for 8 months, the materials could be still readily dissolved in water and producing aqueous IMC nanoparticles dispersion with similar particle size and particle size distribution (Fig. S5).

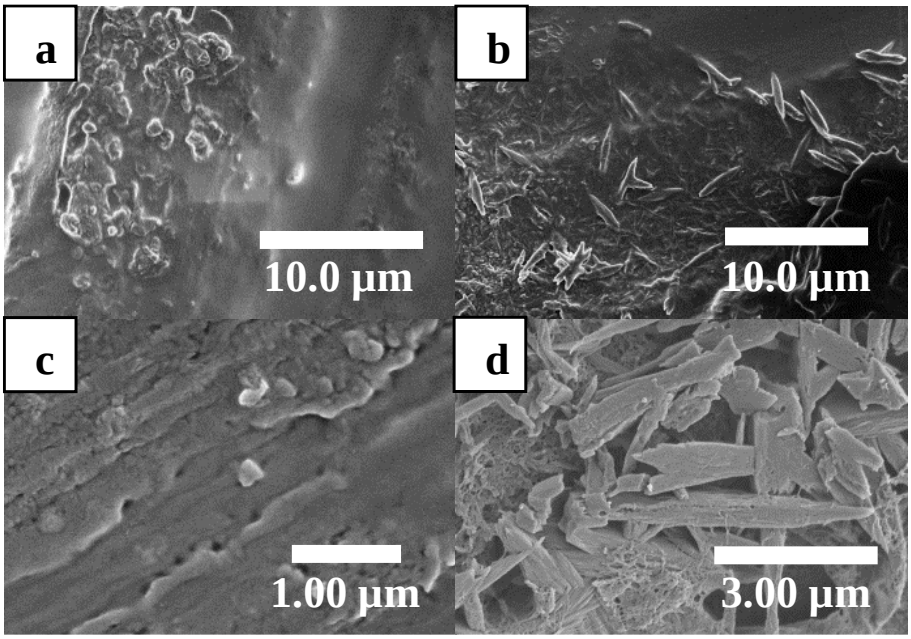

Fig. 8 SEM images of IMC nanoparticles formed from a) 0.6 crosslinked PEG-PNIPAM emulsion with 80% oil phase (W/O=1/4); b) 0.6 crosslinked PEG-PNIPAM emulsion with 75% oil phase

(W/O=1/3); c) 0.6 crosslinked PEG-PNIPAM emulsion with 66% oil phase (W/O=1/2); and d) the precipitated IMC microparticles after centrifuging sample (a).

SEM images of IMC nanoparticles (Fig. 8) were obtained. Fig. 8a and 8c show ellipsoid shaped particles ranging from 300 nm to 1000 nm. This wide range can be explained by comparison with the DLS data in Figure S3a, which showed that particles incorporated within 0.6 crosslinked PEG-NIPAM exhibited a broad size distribution from 100 to 1000 nm. Figure 8b shows needle shaped IMC nanoparticles around 1000 nm, although the same preparation method was used. These findings are considerably different from the measured DLS data. An explanation could be that the nanoparticles started to crystalize while in solution or on the SEM stud during solvent evaporation. Microparticles of IMC were precipitated by centrifugation and observed under SEM as well (Fig. 8d).

SEM imaging of the freeze-dried porous materials was also performed. The highly porous structure was observed for all the samples (Fig. 9 and Fig. S6). Like the porous materials containing OR nanoparticles (Fig. 6), similar droplet templated pores with high interconnectivity could be observed. The pores in Fig. 9b show a diameter range of 2 to 5 µm, similar to the droplet sizes measured in Fig. 7. The polymer scaffold with IMC nanoparticles seemed to be well defined and smooth, while the ridges in Fig. 6 clearly showed a more fibrous structure for the scaffold with OR nanoparticles. As for OR, it was very difficult to observe IMC nanoparticles in the scaffold directly. Changes in crosslinkage or O:W ratio did not change pore size or size distribution significantly, contrary to the previous report [56]. This is likely due to the fact that all emulsions were formed by homogenization in this study, which predominantly influenced droplet shape and size.

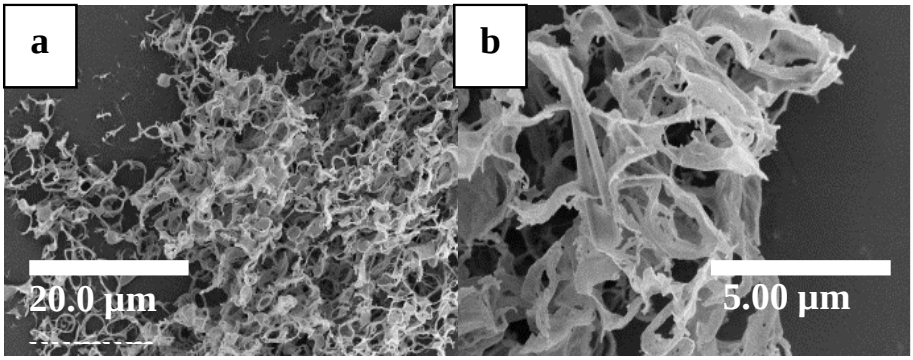

Fig. 9 SEM images of 0.9 crosslinked PEG-PNIPAM scaffold with IMC nanoparticles at different magnifications (a, b). The original emulsion was 75% oil phase.

Generally, amorphous drugs exhibit higher solubility and dissolution rate, which is favourable for drug applications [57]. The crystallinity of IMC nanoparticles was therefore examined. It is known that IMC has more than one polymorphic form. The two most stable ones are α- and γ-IMC, with melting points of 155 °C and 161 °C respectively [58]. PXRD patterns of PEG-PNIPAM, IMC and their composites were recorded and given in Fig. 10. Comparison with predicted PXRD data from single crystal data (Fig. S7) indicated that the IMC used in this study was γ-Indomethacin (Fig. 10b) [59,60]. PXRD data of IMC nanoparticles in 0.3 crosslinked PEG-PNIPASM showed only three sharp peaks at 15 °, 20 ° and 25 ° with low intensity (Fig. 10c), similar to the PXRD pattern of PEG-PNIPAM (Fig. 10a). This suggested that the incorporated IMC nanoparticles were not highly crystalline. Similar patterns were recorded for the IMC particles incorporated into the 0.6 and 0.9 crosslinked PEG-PNIPAM (Fig. S8). Polymers typically form amorphous structures, however semicrystaline structures which exhibit amorphous and crystalline regions are known for polymers as well. Semicrystalinity accounts for the sharp peaks in the PXRD, as well as the broad underlying peak, the so called 'halo', from 15° to 30° (Fig. 10a). In order to identify the phase of IMC particles more clearly, the IMC nanoparticles were separated from the polymer by centrifuging at 13000 rpm for 5 minutes. A control experiment with aqueous polymer solution at this speed showed no precipitation of polymer PEG-PNIPAM. Fig. 10d shows the similar PXRD pattern as Fig. 10c (non-centrifuged), but with the peak intensity significantly decreased. This led us to the conclusion that these peaks were more likely the artefacts of PEG-PNIPAM adsorbed to IMC particles and precipitated together. This indicated that amorphous IMC nanoparticles were produced by this approach.

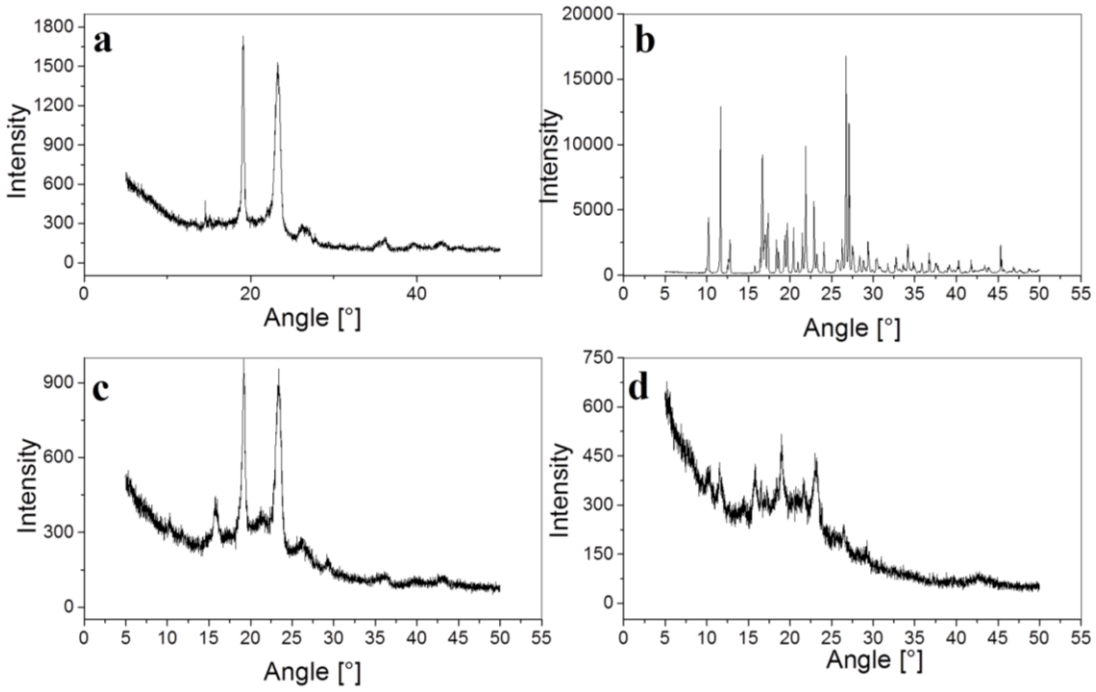

Fig. 10 PXRD patterns of a) raw block copolymer PEG-PNIPAM;b) as-purchased IMC; c) IMC particles with 0.3 crosslinked PEG-PNIPAM; d) IMC nanoparticles obtained after centrifugation of the nanosuspension at 13000 rpm for 5 minutes.

3.4 Further extension to ketoprofen and ibuprofen nanoparticles

In order to demonstrate the versatility of the emulsion-freeze-drying approach, two more drugs, ketoprofen and ibuprofen were processed using the same procedure. Since the highest yield for IMC was achieved using 0.9 crosslinked PEG-PNIPAM and 66 % o-xylene, these conditions were also used for ketoprofen and ibuprofen. It was possible to form stable emulsions with droplet sizes between 5 to 25 µm (Fig. S9, Fig. S10), as already observed for emulsions containing indomethacin (Fig. 7b). After freeze-drying, porous white materials were obtained for both ketoprofen and ibuprofen, which were dissolved in water to produce a clear suspension without any precipitates observed. DLS measurements were performed without any pre-treatment of the nanosuspensions. Zeta potential was quiet similar for both drugs at -8 ± 19 mV (ibuprofen) and – 8 ± 23 mV (ketoprofen). The DLS profiles by intensity (Fig. S11) gave the peak size 198 nm for ibuprofen and 211 nm for ketoprofen. The particle size distribution was calculated to be 1.32 for ketoprofen and 1.15 for ibuprofen. A narrower particle size distribution was observed if the DLS profiles were

plotted by particle number percentage, with the peak size much smaller at 60 nm for ketoprofen and 100 nm for ibuprofen (Fig. S12). This indicates that a 100% yield of nanoparticles for ketoprofen and ibuprofen was achieved by the emulsion-freeze-drying approach.

4 Conclusions

Lightly crosslinked branched block copolymer PEG-PNIPAM has been synthesized. Well-defined nanoparticles could be obtained by mixing its organic solution (*e.g*., tetrahydrofuran, acetone, etc.) and water and followed by evaporation of the organic solvent. The polymer could be easily dissolved in water to get clear solutions with PEG-PNIPAM nanoparticles present. Oil-in-water emulsions were formed using the PEG-PNIPAM nanoparticles as stabilizers. By dissolving hydrophobic dye or poorly water-soluble drugs in the formed oil-in-water emulsion, an emulsion-freeze-drying approach was employed to produce dye/drug nanoparticles *in situ* within the dry porous PEG-PNIPAM scaffolds. The scaffolds prevented aggregation of the dye/drug nanoparticles in solid state and could be readily dissolved in water to generate aqueous nanoparticles dispersion. The use of PEG-PNIPAM as both surfactant and polymeric support is highly efficient and versatile, as demonstrated by the hydrophobic dye Oil Red O and several drugs. The yield of nanoparticles varied but could achieve 100% for both ketoprofen and ibuprofen. Both the block copolymer nanoparticles and the emulsion-freeze-drying approach are highly promising in addressing the poor water solubility problem and potential use in nanomedicine for treatment.

Acknowledgement

UW acknowledges the joint PhD studentship between the University of Liverpool and the A*Star Research Attachment Program (ARAP) scholarship. TH acknowledges the support from NSFC (China, 21574035). The authors are grateful for the access to the facilities in the Centre for Materials Discover and MicroBioRefinary at the University of Liverpool.

References

[1] R.A. Prentis, Y. Lis, S.R. Walker, Pharmaceutical innovation by the seven UK-owned pharmaceutical companies (1964-1985), Br. J. Clin. Pharmacol., 25 (1988) 387-396.

[2] I. Kola, J. Landis, Can the pharmaceutical industry reduce attrition rates?, Nat. Rev. Drug Discov., 3 (2004) 711-716.

[3] N.A. Kasim, M. Whitehouse, C. Ramachandran, M. Bermejo, H. Lennernäs, A.S. Hussain, H.E. Junginger, S.A. Stavchansky, K.K. Midha, V.P. Shah, G.L. Amidon, Molecular properties of WHO essential drugs and provisional biopharmaceutical classification, Mol. Pharm., 1 (2004) 85-96.

[4] G. Amidon, H. Lennernäs, V. Shah, J. Crison, A theoretical basis for a biopharmaceutic drug classification: the correlation of in vitro drug product dissolution and in vivo vioavailability, Pharm. Res., 12 (1995) 413-420.

[5] J. Kreuter, Nanoparticles—a historical perspective, Int. J. Pharm., 331 (2007) 1-10.

[6] G. Kaptay, On the size and shape dependence of the solubility of nano-particles in solutions, Int. J. Pharm., 430 (2012) 253-257.

[7] W. Ostwald, Über die vermeintliche Isomerie des roten und gelben Quescksilberoxyds und die Oberflachenspannung fester Körper, Z. Phys. Chem., 34 (1900) 795-503.

[8] A.A. Noyes, W.R. Whitney, The rate of solution of solid substances in their own solutions, J. Am. Chem. Soc., 19 (1897) 930-934.

[9] E. Merisko-Liversidge, G.G. Liversidge, E.R. Cooper, Nanosizing: a formulation approach for poorly-water-soluble compounds, Eur. J. Pharm. Sci., 18 (2003) 113-120.

[10] E. Merisko-Liversidge, G.G. Liversidge, Nanosizing for oral and parenteral drug delivery: A perspective on formulating poorly-water soluble compounds using wet media milling technology, Adv. Drug Del. Rev., 63 (2011) 427-440.

[11] G.G. Liversidge, K.C. Cundy, J.F. Bishop, D.A. Czekai, Surface modified drug nanoparticles, (January 25, 1991) U.S.Patent 5,145,684 A.

[12] U.P. G. Geetha, K. Arshad Ahmed Khan, Various techniques for preparation of nanosuspension-a review, Int. J. Pharm. Res. Rev., 3 (2014) 30-37.

[13] V.B. Patravale, A.A. Date, R.M. Kulkarni, Nanosuspensions: a promising drug delivery strategy, J. Pharm. Pharmacol., 56 (2004) 827-840.

[14] M.J. Grau, O. Kayser, R.H. Müller, Nanosuspensions of poorly soluble drugs — reproducibility of small scale production, Int. J. Pharm., 196 (2000) 155-159.

[15] L. Gao, D. Zhang, M. Chen, T. Zheng, S. Wang, Preparation and characterization of an oridonin nanosuspension for solubility and dissolution velocity enhancement, Drug Dev. Ind. Pharm., 33 (2007) 1332-1339.

[16] J.-U.A.H. Junghanns, R.H. Müller, Nanocrystal technology, drug delivery and clinical applications, Int. J. Nanomedicine, 3 (2008) 295-310.

[17] C.M. Keck, R.H. Müller, Drug nanocrystals of poorly soluble drugs produced by high pressure homogenisation, Eur. J. Pharm. Biopharm., 62 (2006) 3-16.

[18] B. Sinha, R.H. Müller, J.P. Möschwitzer, Bottom-up approaches for preparing drug nanocrystals: Formulations and factors affecting particle size, Int. J. Pharm., 453 (2013) 126-141.

[19] H.-K. Chan, P.C.L. Kwok, Production methods for nanodrug particles using the bottom-up approach, Adv. Drug Del. Rev., 63 (2011) 406-416.

[20] H. Fessi, F. Puisieux, J.P. Devissaguet, N. Ammoury, S. Benita, Nanocapsule formation by interfacial polymer deposition following solvent displacement, Int. J. Pharm., 55 (1989) R1-R4.

[21] S. Stainmesse, H. Fessi, J.P. Devissaguet, F. Puisieux, C. Theis, Process for the preparation of dispersible colloidal systems of a substance in the form of nanoparticles, (July 28, 1192) U.S. Patent 5,133,908 A.

[22] U. Bilati, E. Allémann, E. Doelker, Development of a nanoprecipitation method intended for the entrapment of hydrophilic drugs into nanoparticles, Eur. J. Pharm. Sci., 24 (2005) 67-75.

[23] R. Fowler, Higee-a status report, Chemical Engineer, (1989) 35-37.

[24] Z.-L. Zhang, Y. Le, J.-X. Wang, H. Zhao, J.-F. Chen, Development of stabilized itraconazole nanodispersions by using high-gravity technique, Drug Dev. Ind. Pharm., 38 (2012) 1512-1520.

[25] E. Reverchon, I. De Marco, E. Torino, Nanoparticles production by supercritical antisolvent precipitation: A general interpretation, J. Supercrit. Fluids, 43 (2007) 126-138.

[26] M. Türk, D. Bolten, Formation of submicron poorly water-soluble drugs by rapid expansion of supercritical solution (RESS): Results for Naproxen, J. Supercrit. Fluids, 55 (2010) 778-785.

[27] J.W. Tom, G.-B. Lim, P.G. Debenedetti, R.K. Prud'homme, Applications of supercritical fluids in the controlled release of drugs, in: E. Kiran, J.F. Brennecke (Eds.) Supercritical Fluid Engineering Science, American Chemical Society, Washington DC, 1992, pp. 238-257.

[28] P. Pathak, M.J. Meziani, T. Desai, Y.-P. Sun, Nanosizing drug particles in supercritical fluid processing, J. Am. Chem. Soc., 126 (2004) 10842-10843.

[29] K. Masters, Spray drying handbook, 3rd ed., John Wiley and Sons, New York, 1979.

[30] B. Bhandari, M.W. Woo, 2.2 Principles of Spray Drying, in: B. Bhandari, N. Bansal, M. Zhang, P. Schuck (Eds.) Handbook of Food Powders: Processes and Properties, Woodhead Publishing, Camebridge, 2014.

[31] K. Rizi, R.J. Green, M. Donaldson, A.C. Williams, Production of pH-responsive microparticles by spray drying: Investigation of experimental parameter effects on morphological and release properties, J. Pharm. Sci., 100 (2011) 566-579.

[32] F. Franks, Freeze-drying of bioproducts: putting principles into practice, Eur. J. Pharm. Biopharm., 45 (1998) 221-229.

[33] W. Abdelwahed, G. Degobert, S. Stainmesse, H. Fessi, Freeze-drying of nanoparticles: Formulation, process and storage considerations, Adv. Drug Del. Rev., 58 (2006) 1688-1713.

[34] J.D. Mellor, Fundamentals of freeze-drying, Academic Press Inc.(London) Ltd., 1978.

[35] Y.-F. Maa, P.-A. Nguyen, T. Sweeney, S.J. Shire, C.C. Hsu, Protein inhalation powders: spray drying vs spray freeze drying, Pharm. Res., 16 (1999) 249-254.

[36] H. Costantino, L. Firouzabadian, K. Hogeland, C. Wu, C. Beganski, K. Carrasquillo, M. Córdova, K. Griebenow, S. Zale, M. Tracy, Protein spray-freeze drying. Effect of atomization conditions on particle size and stability, Pharm. Res., 17 (2000) 1374-1382.

[37] H.R. Costantino, L. Firouzabadian, C. Wu, K.G. Carrasquillo, K. Griebenow, S.E. Zale, M.A. Tracy, Protein spray freeze drying. 2. Effect of formulation variables on particle size and stability, J. Pharm. Sci., 91 (2002) 388-395.

[38] H. Zhang, D. Wang, R. Butler, N.L. Campbell, J. Long, B. Tan, D.J. Duncalf, A.J. Foster, A. Hopkinson, D. Taylor, D. Angus, A.I. Cooper, S.P. Rannard, Formation and enhanced biocidal activity of water-dispersable organic nanoparticles, Nature Nanotechnol., 3 (2008) 506-511.

[39] L. Qian, A. Ahmed, H. Zhang, Formation of organic nanoparticles by solvent evaporation within porous polymeric materials, Chem. Commun., 47 (2011) 10001-10003.

[40] A.D. Roberts, H. Zhang, Poorly water-soluble drug nanoparticles via solvent evaporation in water-soluble porous polymers, Int. J. Pharm., 447 (2013) 241-250.

[41] T. He, D.J. Adams, M.F. Butler, C.T. Yeoh, A.I. Cooper, S.P. Rannard, Direct synthesis of anisotropic polymer nanoparticles, Angew. Chem. Int. Ed., 46 (2007) 9243-9247.

[42] T. He, D.J. Adams, M.F. Butler, A.I. Cooper, S.P. Rannard, Polymer nanoparticles: Shape-directed monomer-to-particle synthesis, J. Am. Chem. Soc., 131 (2009) 1495-1501.

[43] A.W. Jackson, P. Chandrasekharan, J. Shi, S.P. Rannard, C.-T. Yang, T. He, Synthesis and in vivo magnetic resonance imaging evaluation of biocompatible branched copolymer nanocontrast agents, Inter. J. Nanomed., 10 (2015) 5895-5907.

[44] H. Gao, K. Matyjaszewski, Synthesis of molecular brushes by "grafting onto" method: Combination of ATRP and click reactions, J. Am. Chem. Soc., 129 (2007) 6633-6639.

[45] H. Gao, K. Matyjaszewski, Synthesis of star polymers by a combination of ATRP and the "click" coupling method, Macromolecules, 39 (2006) 4960-4965.

[46] K.-Y. Baek, M. Kamigaito, M. Sawamoto, Core-functionalized star polymers by transition metal-catalyzed living radical polymerization. 2. Selective interaction with protic guests via core functionalities, Macromolecules, 35 (2002) 1493-1498.

[47] F.L. Hatton, L.M. Tatham, L.R. Tidbury, P. Chambon, T. He, A. Owen, S.P. Rannard, Hyperbranched polydendrons: a new nanomaterials platform with tuneable permeation through model gut epithelium, Chem. Sci., 6 (2015) 326-334.

[48] A.M. Dwivedi, Residual solvent analysis in pharmaceuticals, Pharm. Technol., 11 (2002) 42-46.

[49] N. Grant, H. Zhang, Poorly water-soluble drug nanoparticles via an emulsion-freeze-drying approach J. Colloid Interface Sci., 356 (2011) 573-578.

[50] D.L. Teagarden, D.S. Baker, Practical aspects of lyophilization using non-aqueous co-solvent systems, Eur. J. Pharm. Sci., 15 (2002) 115-133.

[51] H. Zhang, A.I. Cooper, Synthesis and applications of emulsion-templated porous materials, Soft Matter, 1 (2005) 107-113.

[52] R. Aveyard, B.P. Binks, J.H. Clint, Emulsions stabilised solely by colloidal particles, Adv. Colloid Interface Sci., 100–102 (2003) 503-546.

[53] P.A. Hassan, S. Rana, G. Verma, Making sense of brownian motion: colloid characterization by dynamic light scattering, Langmuir 31 (2015) 3-12.

[54] T. Svedberg, J.B. Nichols, Determination of size and distribution of size of particle by centrifugal methods, J. Am. Chem. Soc., 45 (1923) 2910-2917.

[55] T. Svedberg, H. Rinde, The ultra-centrifuge, a new instrument for the determination of size and distribution of size particle in amicroscopic colloids, J. Am. Chem. Soc., 46 (1924) 2677-2693.

[56] L. Qian, A. Ahmed, A. Foster, S.P. Rannard, A.I. Cooper, H. Zhang, Systematic tuning of pore morphologies and pore volumes in macroporous materials by freezing, J. Mater. Chem., 19 (2009) 5212-5219.

[57] D.Q.M. Craig, P.G. Royall, V.L. Kett, M.L. Hopton, The relevance of the amorphous state to pharmaceutical dosage forms: glassy drugs and freeze dried systems, Int. J. Pharm., 179 (1999) 179-207.

[58] P. Karmwar, J.P. Boetker, K.A. Graeser, C.J. Strachan, J. Rantanen, T. Rades, Investigations on the effect of different cooling rates on the stability of amorphous indomethacin, Eur. J. Pharm. Sci., 44 (2011) 341-350.

[59] X. Chen, K.R. Morris, U.J. Griesser, S.R. Byrn, J.G. Stowell, Reactivity differences of indomethacin solid forms with ammonia gas, J. Am. Chem. Soc., 124 (2002) 15012-15019.

[60] P.J. Cox, P.L. Manson, γ-Indomethacin at 120 K, Acta Cryst., E57 (2003), 986-988.